AD-A150 289 OPTICAL PROCESSING IN RADON SPACE(U) ARIZONA UNIV 1/1
TUCSON OPTICAL SCIENCES CENTER H H BARRETT 15 NOV 84
AFOSR-TR-84-1267 AFOSR-82-0249

UNCLASSIFIED F/G 20/6 NL

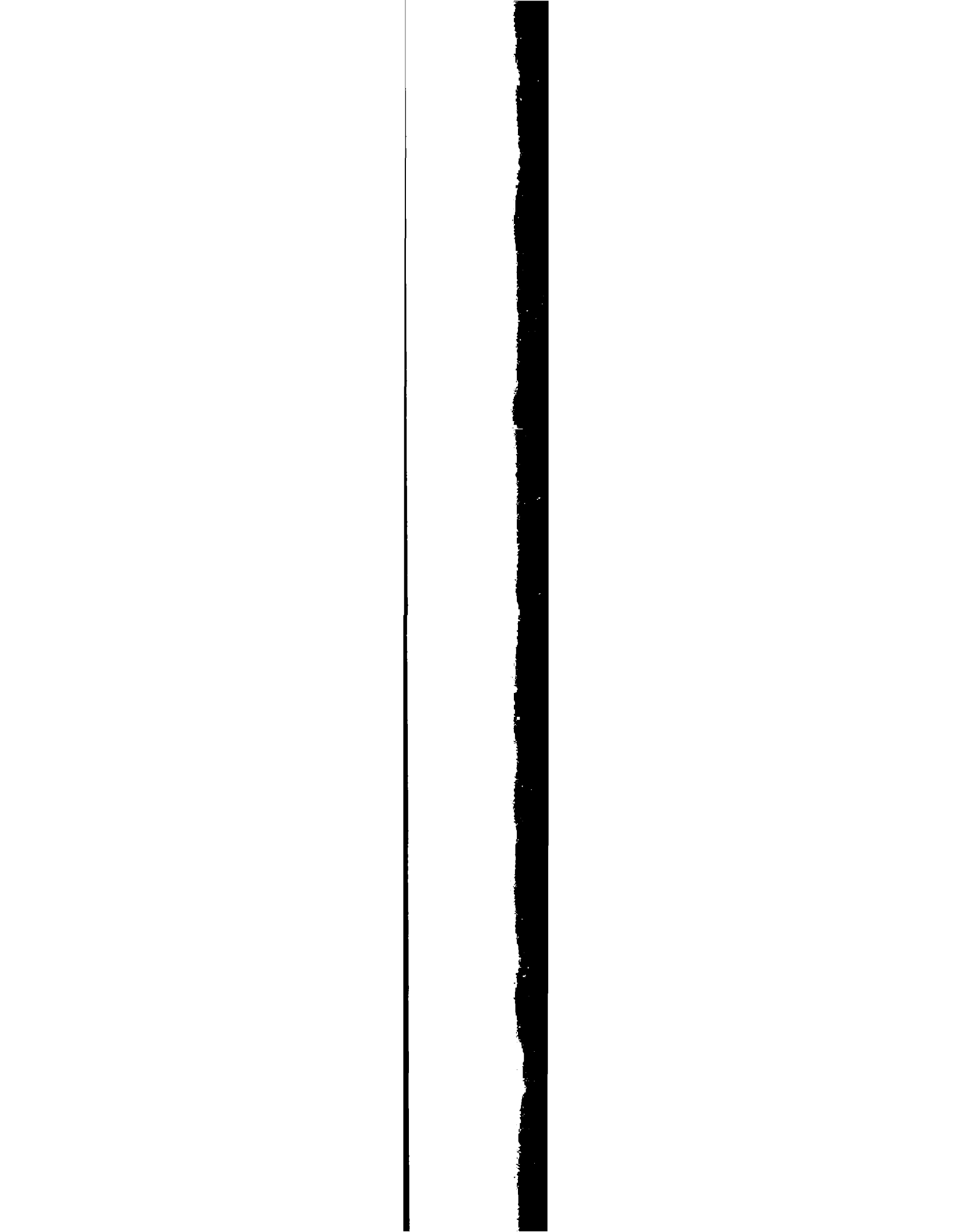

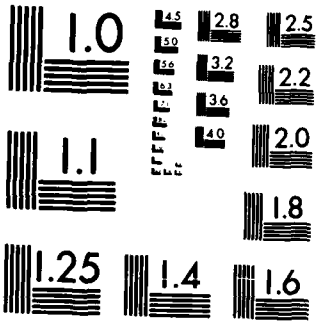

AFOSR-TR- 84-1267

OPTICAL PROCESSING IN RADON SPACE

Harrison H. Barrett
Optical Sciences Center
University of Arizona
Tucson, Arizona 85721

November 15, 1984
Final
~~Annual~~ Report for the Period July 1983 - July 1984

Approved for public release;
distribution unlimited

Prepared for

AIR FORCE OFFICE OF SCIENTIFIC RESEARCH

Unclassified
SECURITY CLASSIFICATION OF THIS PAGE

Carter

REPORT DOCUMENTATION PAGE

1a. REPORT SECURITY CLASSIFICATION: Unclassified	1b. RESTRICTIVE MARKINGS:
2a. SECURITY CLASSIFICATION AUTHORITY:	3. DISTRIBUTION/AVAILABILITY OF REPORT: Approved for public release; distribution unlimited
2b. DECLASSIFICATION/DOWNGRADING SCHEDULE:	
4. PERFORMING ORGANIZATION REPORT NUMBER(S):	5. MONITORING ORGANIZATION REPORT NUMBER(S): AFOSR-TR- 84-1267
6a. NAME OF PERFORMING ORGANIZATION: Optical Sciences Center; 6b. OFFICE SYMBOL (If applicable):	7a. NAME OF MONITORING ORGANIZATION: Air Force Office of Scientific Research
6c. ADDRESS (City, State and ZIP Code): University of Arizona, Tucson, Arizona 85721	7b. ADDRESS (City, State and ZIP Code): Bolling Air Force Base, Washington, D.C. 20332
8a. NAME OF FUNDING/SPONSORING ORGANIZATION: Air Force Off. of Sci. Research; 8b. OFFICE SYMBOL (If applicable):	9. PROCUREMENT INSTRUMENT IDENTIFICATION NUMBER: AFOSR-82-0249
8c. ADDRESS (City, State and ZIP Code): Bolling Air Force Base, Washington, D.C. 20332	10. SOURCE OF FUNDING NOS.

PROGRAM ELEMENT NO.	PROJECT NO.	TASK NO.	WORK UNIT NO.
61102F	2305	B1	

11. TITLE (Include Security Classification): Optical Processing in Radon Space

12. PERSONAL AUTHOR(S): Harrison H. Barrett

13a. TYPE OF REPORT	13b. TIME COVERED	14. DATE OF REPORT (Yr., Mo., Day)	15. PAGE COUNT
~~Annual~~ Final, July 1983-84	FROM 7-83 TO 7-84	84-11-15	20

16. SUPPLEMENTARY NOTATION

17. COSATI CODES			18. SUBJECT TERMS (Continue on reverse if necessary and identify by block number)
FIELD	GROUP	SUB. GR.	Optical data processing, Radon transform, Surface acoustic wave filters

19. ABSTRACT (Continue on reverse if necessary and identify by block number)

Signals of M dimensions (M>1) can be reduced to one-dimensional data by integration over M-1 dimensions. This operation is known as the Radon transform. Many useful two-dimensional signal processing operations can be performed rapidly by first producing the one-dimensional projection data and operating on the projections with efficient one-dimensional processors, such as surface acoustic wave devices. Such operations as spectrum analysis, complex Fourier transformation, production of the Wigner distribution function, and convolution can be performed in this manner, and may be done more rapidly or more accurately than by more conventional methods. Progress in research in this field is reported.

20. DISTRIBUTION/AVAILABILITY OF ABSTRACT	21. ABSTRACT SECURITY CLASSIFICATION
UNCLASSIFIED/UNLIMITED ☒ SAME AS RPT ☐ DTIC USERS ☐	Unclassified

22a. NAME OF RESPONSIBLE INDIVIDUAL	22b. TELEPHONE NUMBER (Include Area Code)	22c. OFFICE SYMBOL
Floyd Lance	(602) 621-6996	

DD FORM 1473, 83 APR — EDITION OF 1 JAN 73 IS OBSOLETE.

Unclassified
SECURITY CLASSIFICATION OF THIS PAGE

1. INTRODUCTION

The Radon transform is well-known as the basis for medical computed tomography, which produces a two-dimensional (2-D) map of x-ray attenuation coefficient within the body from 1-D projection data. The general Radon transform operates on a data set of M-dimensions, reducing the data to a sequence of 1-D data via integration over (M-1) dimensions. The existence of very efficient 1-D signal processing components, such as surface acoustic wave (SAW) filters or charge-coupled devices (CCDs), makes the reduction in dimensionality very useful for many processing applications. Many operations can be performed rapidly on 2-D or 3-D data by performing the Radon transform and processing in 1-D with these sophisticated processors. Such operations as Fourier transformation, convolution, correlation, bandwidth compression, and computation of image moments, ambiguity functions or Wigner distribution functions can be carried out in this manner.

This document is a report of technical progress made during the second year of a proposed three-year program to investigate the application of the Radon transform to signal processing. The stated goals of the program are:

(1) theoretical investigation of the role of the Radon transform in signal processing;

(2) construction of a practical system for 2-D spectral analysis and image filtering at rates of at least 30 frames per second;

(3) proof-of-principle experiments for other processing operations;

(4) determination of the feasibility of 3-D Radon processing.

In the second year, the specific research tasks to be performed were:

(1) continue theoretical analysis of the Radon transform and its applications in signal processing;

(2) finish construction and testing of an optical Radon transformer based on a flying-line scanner;

(3) complete construction and testing of a SAW Fourier transformer including demonstration of the ability to compute complex transforms;

(4) use the optical Radon transformer and SAW Fourier transformer for 2-D spectrum analysis;

(5) design and construct an optical back-projector;

(6) design a SAW filter with a $|\nu|$-filter;

(7) begin construction and testing of the $|\nu|$-filter;

(8) investigate the feasibility of 3-D data-processing systems based on spectral hole burning;

(9) study the performance of a Radon correlation tracker by computer simulation;

(10) demonstrate the principle of the correlation tracker with a breadboard experiment.

2. STATUS OF THE RESEARCH

Progress made toward accomplishing the specific goals for the second year is as follows:

2.1 Theoretical investigation of the Radon transform applied to signal processing.

The work in this area has concentrated on the Wigner distribution function (WDF). The WDF, a simultaneous coordinate-frequency representation of a function, has applications in system description and pattern recognition. Because it is computationally demanding, it is not often implemented digitally, especially for 2-D input data. Several systems have been proposed to compute the WDF optically: either the full 2-D function of 1-D input data or 2-D slices of the 4-D function of 2-D input data. We have shown that the Radon transform is an effective tool for calculating the WDF because of the reduction to a sequence of 1-D Fourier transforms of an easily generated function. The output data can take the form of either 1-D lines or 2-D slices of the 4-D WDF. We have successfully implemented this operation and published the results in Optical Engineering. Investigation and implementation of other operations in Radon space, such as 2-D scale invariant pattern recognition and 2-D cepstrum analysis, is continuing.

2.2 Completion of the optical Radon transformer.

All of the experimental work completed thus far has been accomplished using one version of the flying-line scanner, shown schematically in Fig. 1. It produced a line of He-Ne laser light with an anamorphic optical system and projected the line onto the input data plane. An acousto-optic Bragg cell driven by a voltage-controlled oscillator enabled the line to be scanned across the data plane, resolving approximately 150 lines in an aperture of 30 mm diameter. A single scan was performed in 10_{μ} s, yielding one line through the Radon transform of the input data. The azimuth of the scan angle could be varied with an image-rotation prism, allowing the complete Radon transform to be generated. The time required to produce the transform is limited by the rotation speed of the prism to approximately 0.5 Hz, but a new prism system now under construction will achieve the required 7.5-Hz rotation rate, giving a 30-Hz frame rate. The first version of the optical Radon transformer wasted much light, requiring a photomultiplier detector. A new, efficient, and compact system has been built, allowing the use of a fast P-I-N photodiode detector and making computation of complex Fourier transforms more convenient.

2.3. Completion of the SAW chirp Fourier transformer.

Production of 1-D power spectra with a SAW Fourier transformer was easily done, but implementation of the complete 1-D complex Fourier transform was more difficult because of the accurate timing required.

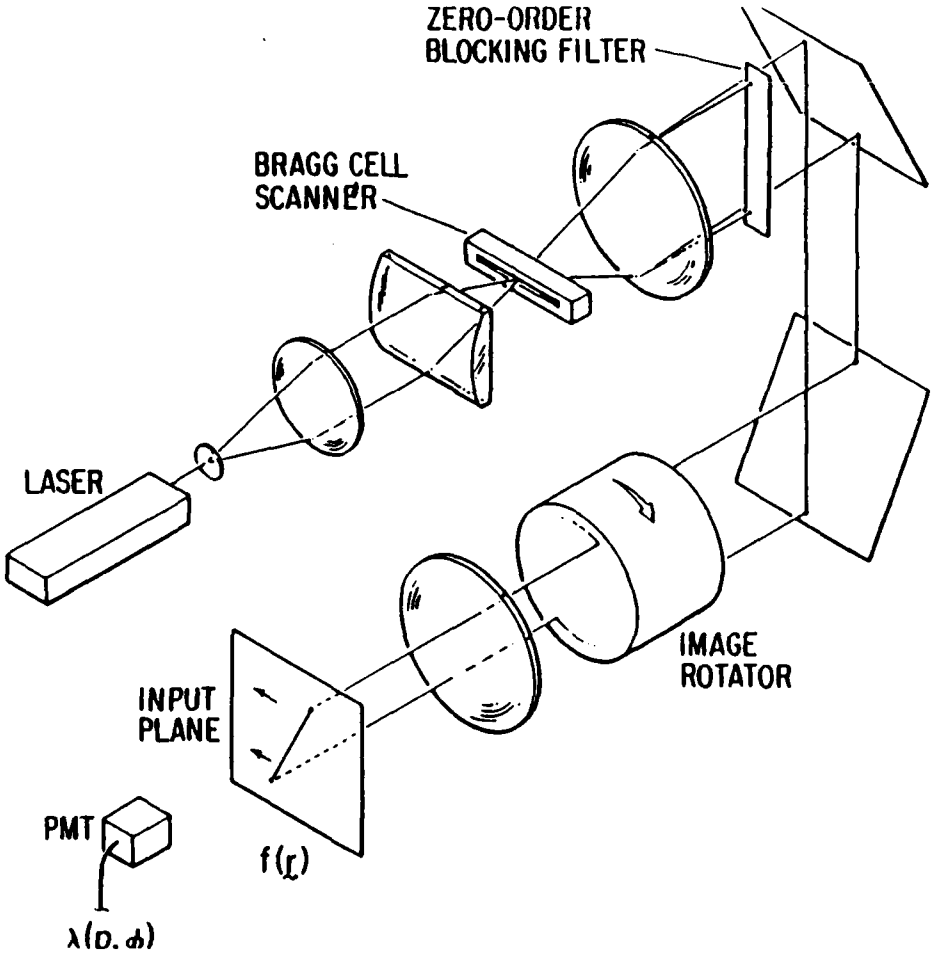

1. Flying-Line Scanner. The laser source is imaged to a line on the input plane by the cylindrical lens. The Bragg cell is driven by a chirp signal from a voltage-controlled oscillator, producing a phase grating of linearly varying frequency that scans the line across the input. The light transmitted or reflected from the input is collected by the detector. One scan across the input produces one projection of the Radon transform. Rotation of the scan azimuth by the prism allows the production of the complete Radon transform.

This problem has been solved, and we are now able to generate the complex Fourier transform of real input data. Analog signals that are 10 μ s long can be transformed in less than 30 μ s, yielding the real and imaginary parts of the Fourier transform (i.e., sine and cosine transform respectively) in separate channels. A schematic diagram of the complex SAW chirp Fourier transformer is shown in Fig. 2. The resolution of the transform is limited to 50 data points by the time-bandwidth product of one of the SAW chirp filters. Results of the transformation of a sequence of 1-D scans are shown in Fig. 3, along with a computer simulation. Performance of the transformer is seen to be excellent.

2.4. Generation of 2-D spectra with the system.

Using the optical Radon transformer and SAW chirp Fourier transformer, 2-D power spectra have been produced for several objects, both transmissive and reflective. Selected results are presented in Fig. 4. In addition, the technique has been applied to a simulation of Labeyrie stellar speckle interferometry, by averaging a sequence of simulated stellar speckle patterns to produce diffraction-limited information (i.e., the autocorrelation) of the original source. This work has also been published in Optical Engineering.

2.5. Construction of the optical back-projector.

The optical back-projector is composed of two distinct parts: the high-pass filter and the optical projection system. The optical projector is simple, straightforward, and has been previously

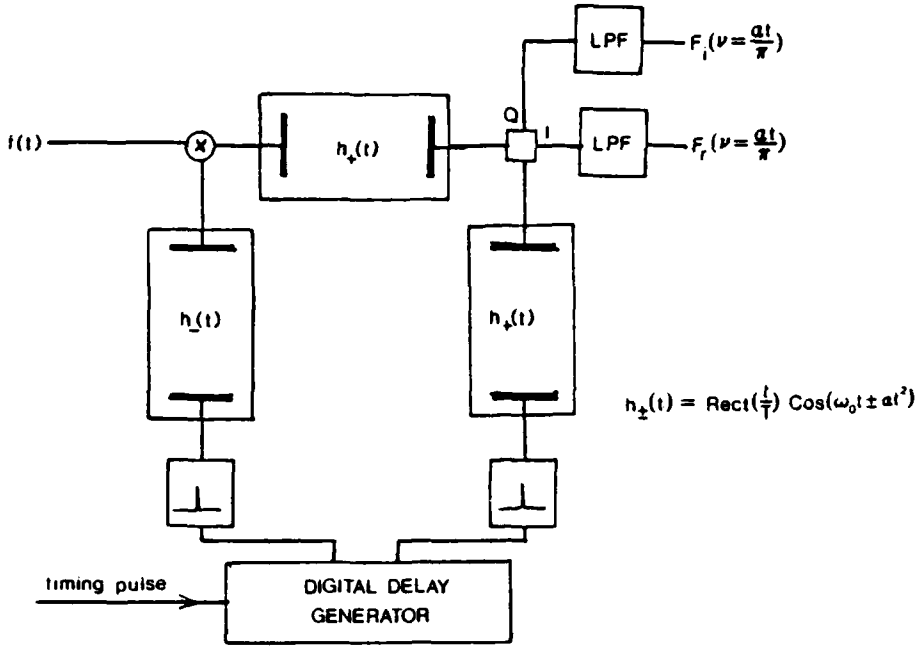

2. Complex SAW Chirp Fourier Transformer. The major components of the SAW transformer are the three SAW chirp filters. The impulse response of such a filter is $h(t) = \mathrm{Rect}(t/T)\ \cos(\omega_0 t \pm \alpha t^2)$. Taking the plus sign in the cosine term yields an upchirp (output frequency increases with time), while the chirp with the negative sign is a downchirp. To produce the complex Fourier transform, the input signal is multiplied by a downchirp in an rf mixer. The product is applied to a filter with an upchirp impulse response. Square-law detection of the output signal yields the squared-modulus of the Fourier transform. Post-multiplication of the filtered signal with a second upchirp in a phase comparator gives, after low-pass filtering, the real and imaginary parts of the Fourier transform (i.e., the cosine and sine transform respectively). Of course, the finite windows of the chirps limit the extent of the Fourier spectrum that is computed as well as the resolution obtainable.

SCANNER OUTPUT AND TRANSFORMS

COMPUTER SIMULATION

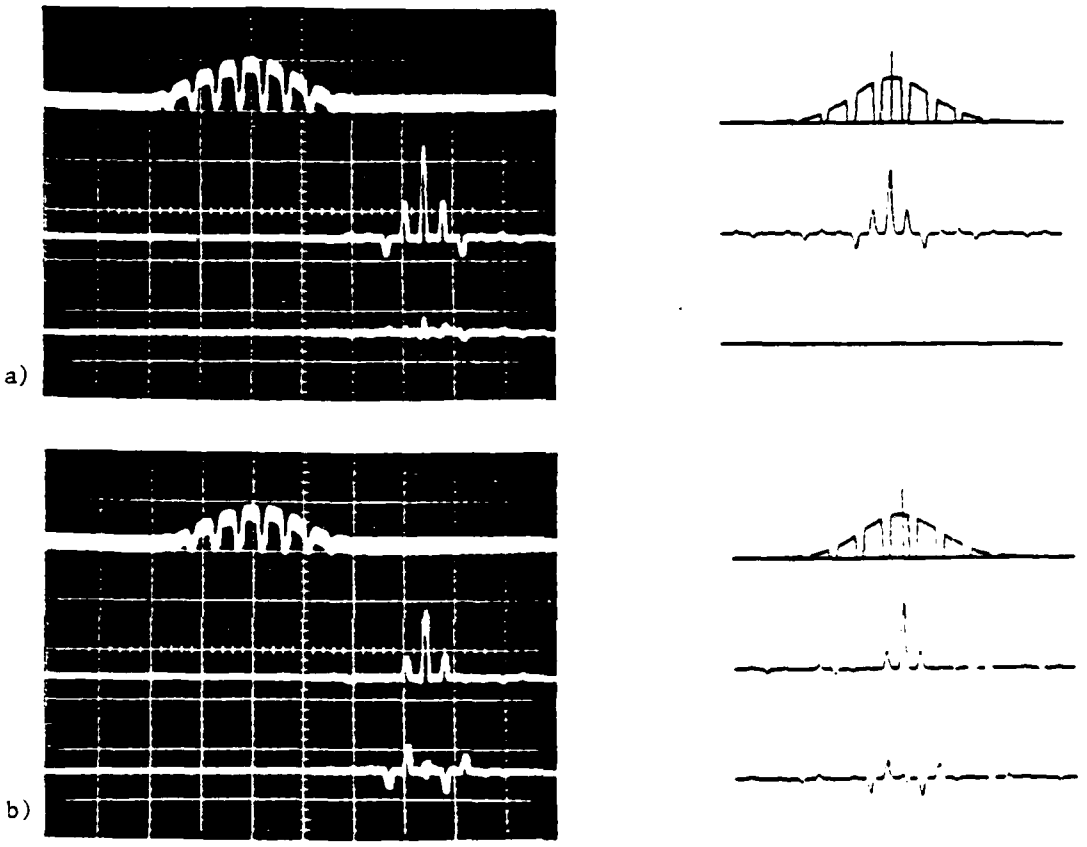

3. One-dimensional complex Fourier transforms with the SAW transformer. This is a sequence of four signals and complex transforms from the SAW transformer, along with computer simulations. The object was a grating (75% transparent, 25% opaque) in a circular aperture of 20-mm diameter. In each case, the first trace is the output of the flying-line scanner, i.e., one projection of the Radon transform. The second and third traces are the cosine and sine transform outputs, respectively, of the SAW complex chirp transformer. a) The grating was centered in the circular aperture, giving a symmetric object yielding a purely real transform, i.e., the sine transform vanishes. In b) , c), and d), the grating was translated incrementally in the aperture, producing a nonzero sine transform. Comparison of each case with the computer simulations shows excellent agreement.

SCANNER OUTPUT AND TRANSFORMS

COMPUTER SIMULATION

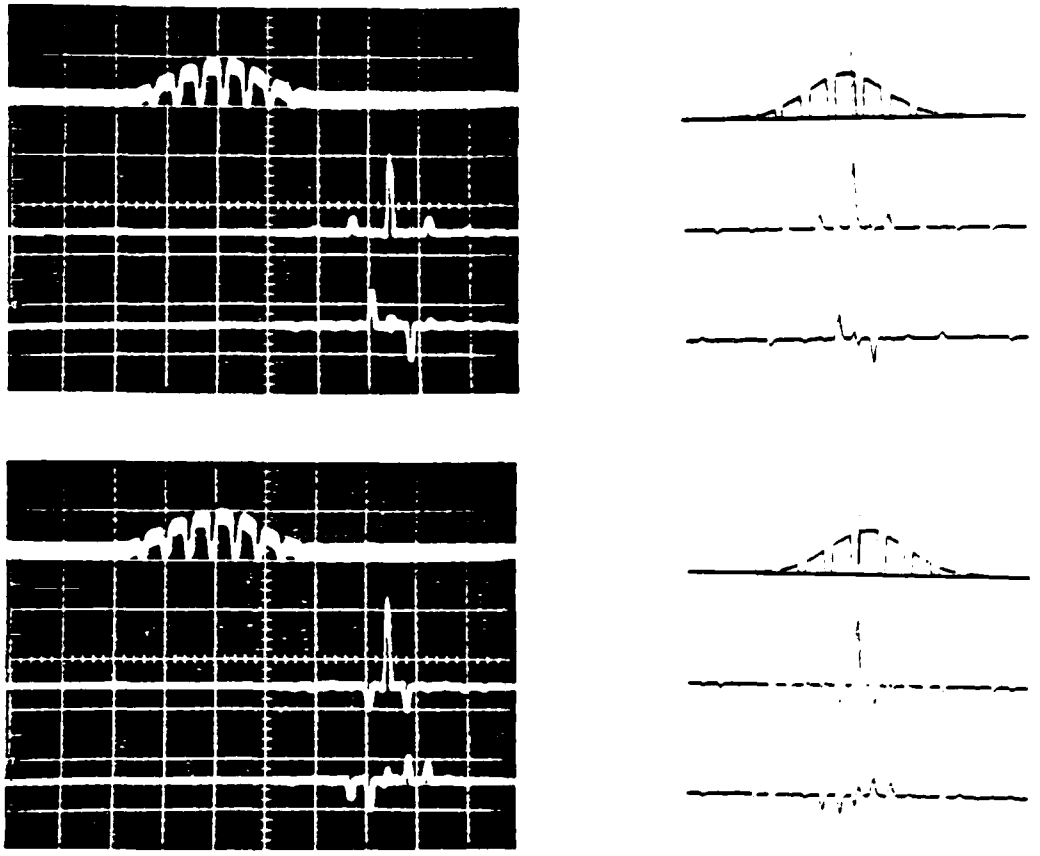

c)

d)

3. One-dimensional complex Fourier transforms with the SAW transformer. This is a sequence of four signals and complex transforms from the SAW transformer, along with computer simulations. The object was a grating (75% transparent, 25% opaque) in a circular aperture of 20-mm diameter. In each case, the first trace is the output of the flying-line scanner, i.e., one projection of the Radon transform. The second and third traces are the cosine and sine transform outputs, respectively, of the SAW complex chirp transformer. a) The grating was centered in the circular aperture, giving a symmetric object yielding a purely real transform, i.e., the sine transform vanishes. In b) , c), and d), the grating was translated incrementally in the aperture, producing a nonzero sine transform. Comparison of each case with the computer simulations shows excellent agreement.

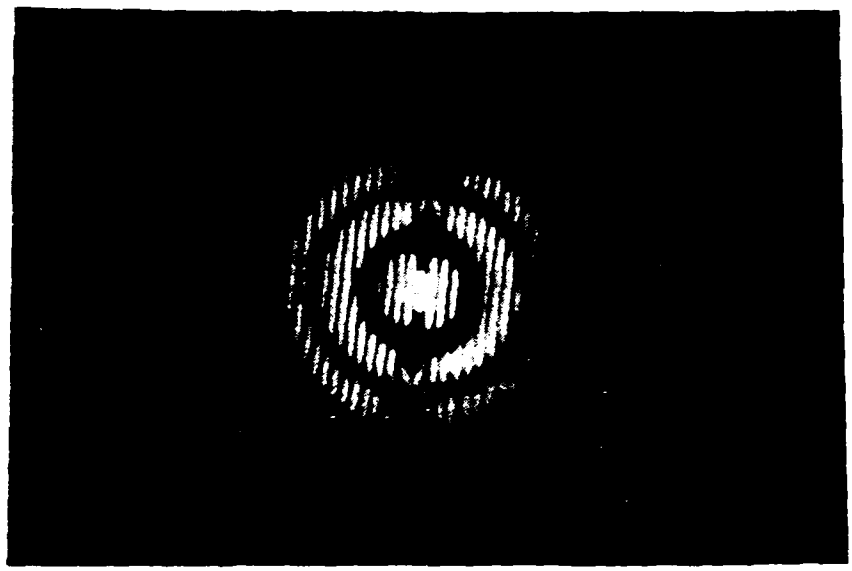

4a. The object was a pair of identical circular apertures, and the cosine fringes across the Airy disk pattern are clearly seen.

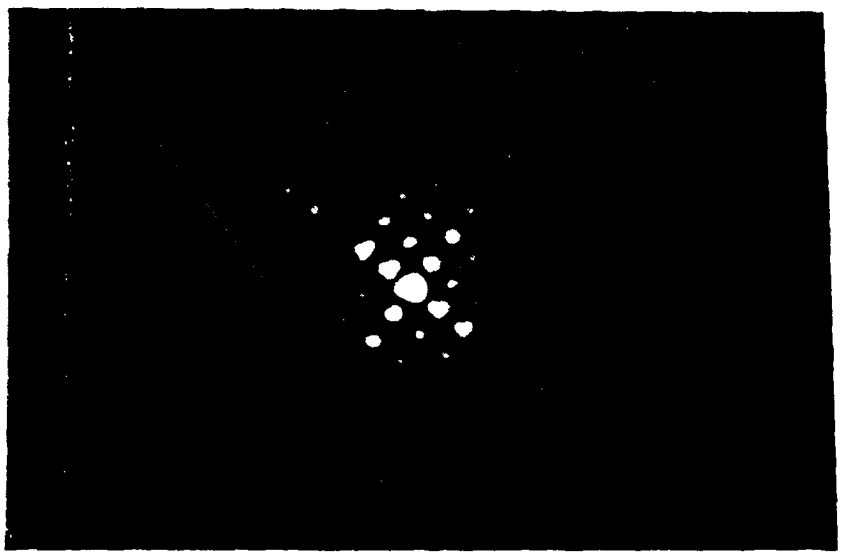

4b. The object consisted of two identical gratings crossed at 90°. The fundamental orders of each grating and the cross-terms are clearly seen.

4. Two-dimensional spectra obtained with the Radon-Fourier transformer. Five examples of two-dimensional spectra are shown. Figures a) to c) show the power spectrum of the object (i.e., squared-magnitude of the Fourier transform), and d) and e) are complex transforms.

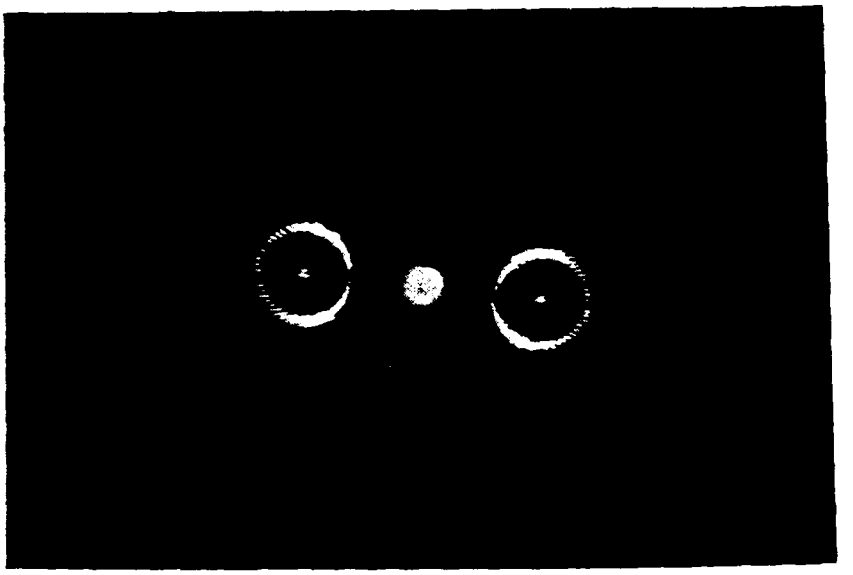

4c. The object whose transform is shown in c) was a computer-generate hologram. The impulse response of the hologram is an annulus, as clearly shown.

4. Two-dimensional spectra obtained with the Radon-Fourier transforme Five examples of two-dimensional spectra are shown. Figures a) t(c) show the power spectrum of the object (i.e., squared-magnitude c the Fourier transform), and d) and e) are complex transforms.

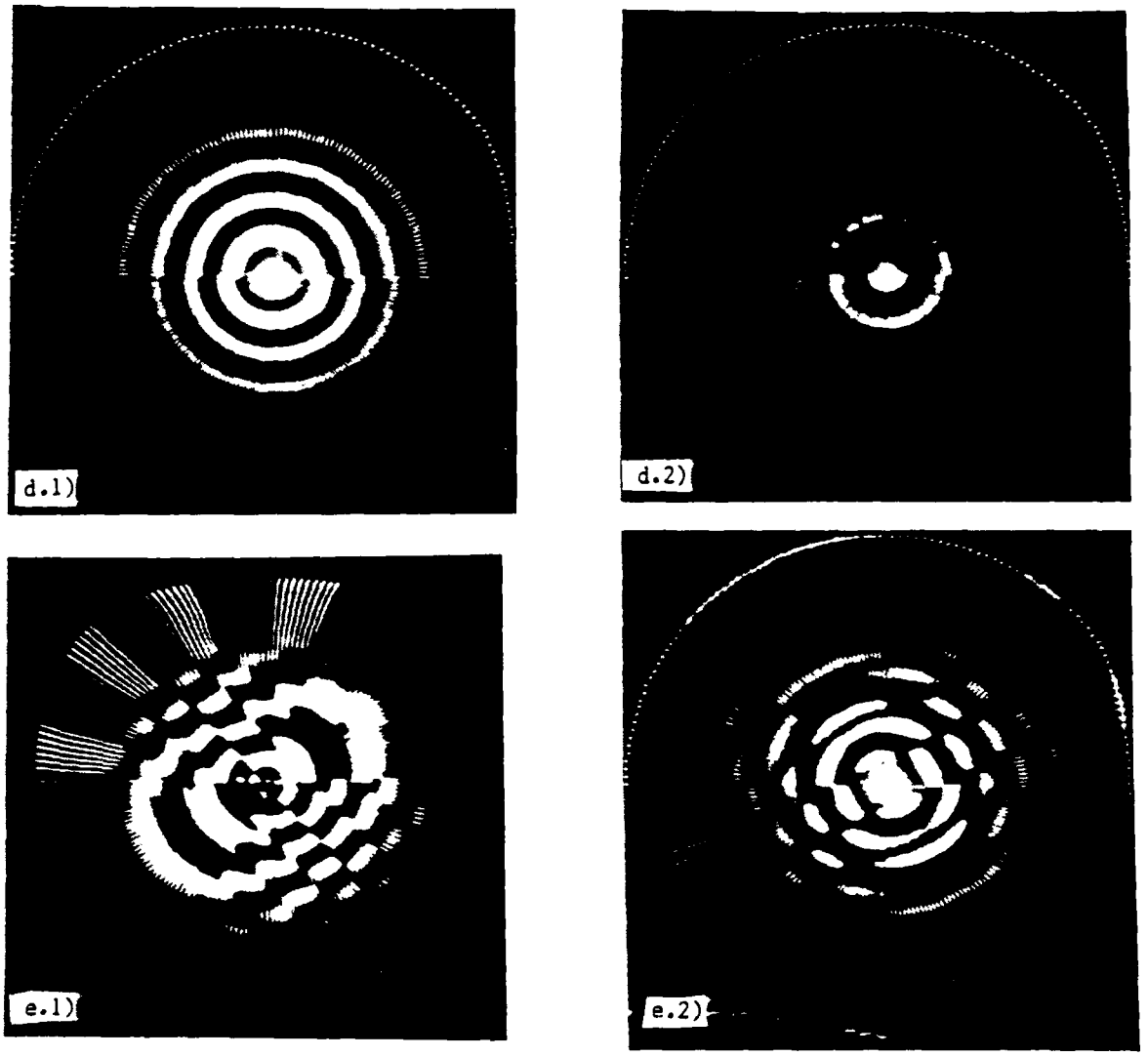

4d. and e. The positive parts of the cosine and sine transforms of a single circular aperture are shown. d) The object is centered in the flying-line scanner, yielding a purely real Fourier transform. In d.1), the positive part of the cosine transform shows the Airy pattern, while in d.2), the sine transform is nearly zero. e) The aperture has been translated in the scanner, yielding a linear phase term and a nonzero sine transform. In e.1), the cosine transform is seen to be symmetric and the fringes due to the linear phase term are shown. The sine transform in e.2) is antisymmetric.

4. Two-dimensional spectra obtained with the Radon-Fourier transformer. Five examples of two-dimensional spectra are shown. Figures a) to c) show the power spectrum of the object (i.e., squared-magnitude of the Fourier transform), and d) and e) are complex transforms.

demonstrated. The high-pass, or $|\nu|$-filter, can be implemented in several ways; the most desirable is a custom-designed SAW filter. This approach will be discussed below. Another feasible method utilizes a SAW convolver with the filter function stored in a fast digital memory. This technique has been tested with a prototype digital memory at low data rates and been found to work satisfactorily. However, at the speeds required for video-rate operation, the digital memory is far too noisy. Components for an improved memory using emitter-coupled logic (ECL) are on order and should solve the problem.

2.6 and 2.7. Design and Construction of SAW $|\nu|$-filter.

The basic design for the SAW $|\nu|$-filter required for the optical back-projector has been completed. It will consist of two SAW filters on the same substrate. Both filters will utilize chirped transducers, oriented to obtain a non-dispersive output. To obtain the required transfer function, two filter outputs will be needed: a triangular bandpass will be subtracted from a rectangular bandpass. A schematic diagram of the filter is shown in Fig. 5. The preliminary test masks for the photolithography have been produced, and the first test filter is being constructed.

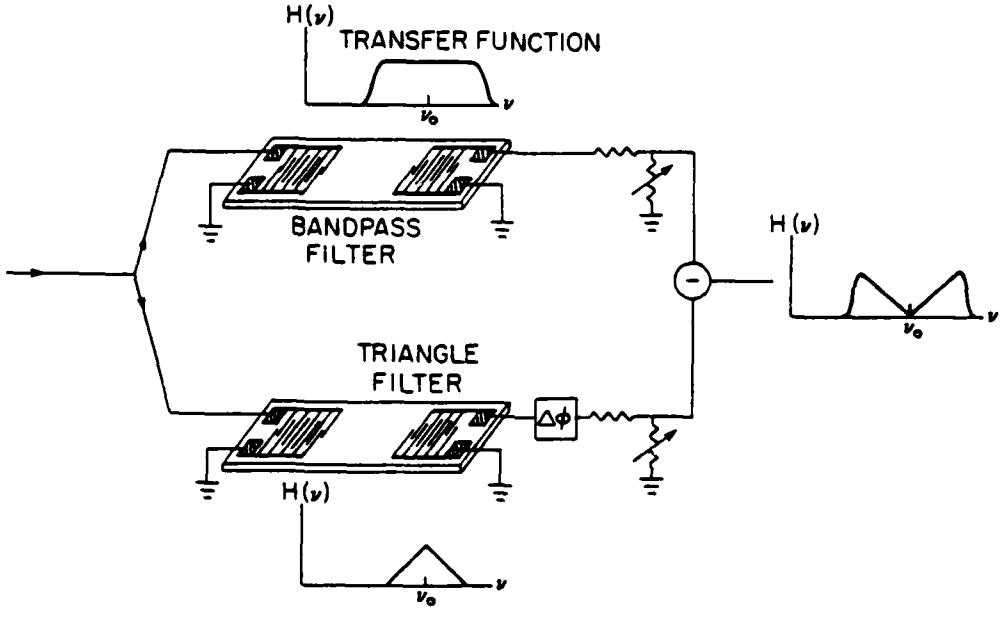

5. Schematic diagram of the surface acoustic wave $|\nu|$-filter. To allow for accurate nulling at the center frequence, the filter is divided into two parts. The incoming signal is split, with half applied to a filter with a triangular transfer function and half to a filter with a near-rectangular passband. A hybrid phase-shifter in one arm compensates for differential phasing in the SAW filters. The outputs are subtracted in a 180° hybrid. The output transfer function has the required shape.

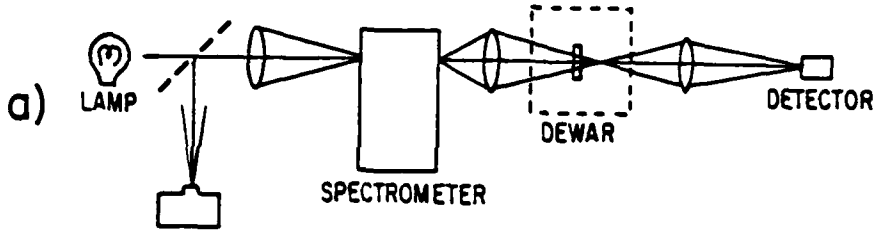

6a. Optical layout for the system to store optical analog data via spectral hole burning.

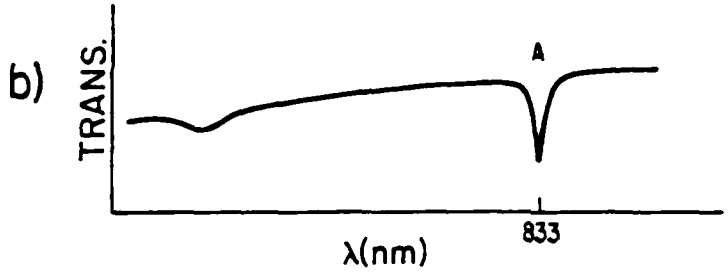

6b. Sample transmission spectrum obtained for a line to be used for storage (λ=833 nm).

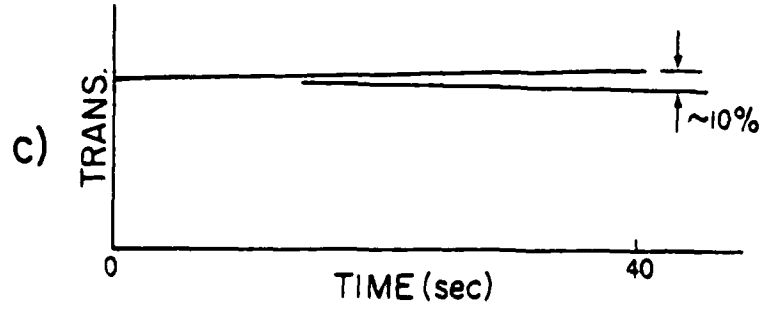

6c. Transmission of the absorption as a function of time during burn. The rise in transmission is due to depletion of the ground state population.

2.8. Investigate the feasibility of 3-D data-processing systems based on spectral hole burning.

The goal for the second year in terms of optical storage of analog data was to demonstrate wavelength-multiplexed storage in alkali-halide crystals. We have investigated wavelength tuning capabilities of laser diodes and test-irradiated a crystal of lithium fluoride (LiF) to observe spectral hole-burning. The optical and electronic systems are not yet in their final forms, but early results are promising. The optical system is shown in Fig. 6a. Using the lamp source alone, we have observed the absorption line to be used for storage, designated as A in Fig. 6b. Tuning the laser diode to a wavelength within the absorption line and recording the transmission as a function of time, we have observed the burning of a hole as shown in Fig. 6c. The increase in transmission was about 10% in 40 secs of exposure. No attempts have been made to determine how much of the laser power is passing through the spectrometer slit, but we expect to be able to increase the burning rate significantly by modifying the optical system to ensure that all the power reaches the crystal.

We have also used the laser-diode drive current to scan the wavelength through the spectrum surrounding the burned hole. Because of the small depth of the hole and the fairly insensitive detector electronics, we were unable to observe conclusively the presence of the burnt hole. We are currently developing improved detector circuitry to reduce the amplifier noise, and are using derivative spectroscopy, rather

than less sensitive transmission spectroscopy, to observe the holes. This should allow us to easily read hole depths of the magnitude we will be writing.

2.9. Study the performance of a Radon correlation-tracker by computer simultation.

2.10. Demonstrate the correlation-tracker with a breadboard experiment.

We have found published results of work very similar to that which we planned to do (Yao and Adrian, Appl. Opt., 23, 1687, 1984), and so we concentrated efforts in another area instead. We have determined that it is feasible to partially perform some operations during the scanning operation. For example, differentiation of the input data could be done by scanning with a Laplacian operator and back-projecting. The Laplacian operator could be generated by using three side-by-side light sources in the scanner, with the center source twice as bright and 180° out-of-phase relative to the other two sources. Suitable sources include laser diodes, but the available wavelengths (>750 nm) are too long to be used with our Bragg cell scanner. Light-emitting diodes exist with suitable wavelengths, but the maximum modulation speed is not sufficient for our purpose. A third possibility is to use the He-Ne laser in the scanner now, with fiber optic delay lines to properly phase the sources. This approach to image differentiation should be less sensitive to noisy data because of the line-integral of the Radon transform.

3. LIST OF PERSONNEL

H.H. Barrett, Principal Investigator, Optical Sciences Center and Department of Radiology, University of Arizona.

Paul Atcheson, Graduate Research Associate.

Roger Easton, Jr., Graduate Research Associate.

Anthony Ticknor, Graduate Research Assistant.

4. PUBLICATIONS RESULTING FROM AFOSR SUPPORT DURING THE SECOND YEAR OF THE PROGRAM

R.L. Easton, Jr., A.J. Ticknor, and H.H. Barrett, "Application of the Radon transform to optical production of the Wigner distribution function," Opt. Eng. 23(6),1984.

A.J. Ticknor, R.L. Easton, Jr., and H.H. Barrett, "A Two-Dimensional Radon-Fourier Transformer," Opt. Eng. 24(1), 1985.

5. PAPERS PRESENTED AT TECHNICAL MEETINGS

A.J. Ticknor, R.L. Easton, Jr. and H.H. Barrett, "High-speed processing of 2-D data via the Radon transform," presented at the 1984 Annual Meeting of the Optical Society of America, San Diego.

R.L. Easton, Jr., A.J. Ticknor, and H.H. Barrett, Processing of 2-D data via the Radon transform II: Applications," presented at the 1984 Annual Meeting of the Optical Society of America, San Diego.

6. FIGURE CAPTIONS

1. Flying-Line Scanner. The laser source is imaged to a line on the input plane by the cylindrical lens. The Bragg cell is driven by a chirp signal from a voltage-controlled oscillator, producing a phase grating of linearly varying frequency that scans the line across the input. The light transmitted or reflected from the input is collected by the detector. One scan across the input produces one projection of the Radon transform. Rotation of the scan azimuth by the prism allows the production of the complete Radon transform.

2. Complex SAW Chirp Fourier Transformer. The major components of the SAW transformer are the three SAW chirp filters. The impulse response of such a filter is $h(t) = \mathrm{Rect}(t/T) \cos(\omega_0 t \pm \alpha t^2)$. Taking the plus sign in the cosine term yields an upchirp (output frequency increases with time), while the chirp with the negative sign is a downchirp. To produce the complex Fourier transform, the input signal is multiplied by a downchirp in an rf mixer. The product is applied to a filter with an upchirp impulse response. Square-law detection of the output signal yields the squared-modulus of the Fourier transform. Post-multiplication of the filtered signal with a second upchirp in a phase comparator gives, after low-pass filtering, the real and imaginary parts of the Fourier transform (i.e., the cosine and sine transform respectively). Of course, the finite windows of the chirps limit the extent of the Fourier spectrum that is computed as well as the resolution obtainable.

3. 1-D Complex Fourier Transforms with the SAW Transformer. This is a sequence of four outputs from the flying line scanner together with the outputs of the chirp Fourier transformer. The left hand figures are the oscilloscope traces from the scan and transformer, while those on the right are computer simulations to demonstrate the accuracy of the computation. The object was a grating (75% transparent, 25% opaque) in a circular aperture. a) The output of the flying line scanner, i.e., one projection of the Radon transform. b) The cosine and sine transforms of the projection with the grating centered in the aperture, resulting in a symmetric object with a purely real transform, i.e., the sine transform vanishes. c) Examples of the cosine and sine transforms of the projection with the grating translated incrementally in the aperture, adding an antisymmetric part to the object, and resulting in a nonzero sine transform. Comparison with the computer simulations shows excellent agreement.

4. 2-D Spectra obtained with the Radon-Fourier Transformer. Five examples of 2-D spectra are shown. a), b), and c) are the squared moduli of the Fourier transform of the object, while d) and e) are complex transforms. a) A pair of identical circular apertures. The cosine fringes across the Airy disc pattern are clearly seen. b) The two gratings crossed at 90°, showing the fundamental orders for both gratings, plus the cross-terms. c) A computer-generated hologram whose impulse response was an annulus. d) and e) Examples of a single circular aperture. In d) the aperture was centered in the flying-line scanner, so that the complex transform is purely real. By translating the object in the flying-line scanner, a linear phase is added to the transform. The sine transform is now nonzero, and both the cosine and sine transforms show fringes.

5. Schematic diagram of the surface acoustic wave $|\nu|$-filter. To allow for accurate nulling at the center frequence, the filter is divided into two parts. The incoming signal is split, with half applied to a filter with a triangular transfer function and half to a filter with a near-rectangular passband. A hybrid phase-shifter in one arm compensates for differential phasing in the SAW filters. The outputs are subtracted in a 180° hybrid. The output transfer function has the required shape.

6a. Optical layout for the system to store optical analog data via spectral hole burning.

6b. Sample transmission spectrum obtained for a line to be used for storage (λ=833 nm).

6c. Transmission of the absorption as a function of time during burn. The rise in transmission is due to depletion of the ground state population.

END

FILMED

3-85

DTIC